Phys. Med. Biol. **43** (1998) 1285–1302. Printed in the UK PII: S0031-9155(98)83675-0

Comparison of finite-difference transport and diffusion calculations for photon migration in homogeneous and heterogeneous tissues

Andreas H Hielscher†‡, Raymond E Alcouffe§ and Randall L Barbour‖

† Bioscience and Biotechnology, CST-4, MS E535, Los Alamos National Laboratory, Los Alamos, NM 87545, USA

§ Transport Methods, XTM, MS B226, Los Alamos National Laboratory, Los Alamos, NM 87545, USA

‖ State University of New York Health Science Center at Brooklyn, Department of Pathology, Box 25, Brooklyn, NY 11203, USA

Received 24 April 1997, in final form 9 November 1997

Abstract. We analyse the limits of the diffusion approximation to the time-independent equation of radiative transfer for homogeneous and heterogeneous biological media. Analytical calculations and finite-difference simulations based on diffusion theory are compared with discrete-ordinate, finite-difference transport calculations. The influence of the ratio of absorption and transport scattering coefficient (μ_a/μ_s') on the accuracy of the diffusion approximation are quantified and different definitions for the diffusion coefficient, D, are discussed. We also address effects caused by void-like heterogeneities in which absorption and scattering are very small compared with the surrounding medium. Based on results for simple homogeneous and heterogeneous systems, we analyse diffusion and transport calculation of light propagation in the human brain. For these simulations we convert density maps obtained from magnetic resonance imaging (MRI) to optical-parameter maps (μ_a and μ_s') of the brain. We show that diffusion theory fails to describe accurately light propagation in highly absorbing regions, such as haematoma, and void-like spaces, such as the ventricles and the subarachnoid space.

1. Introduction

The diffusion approximation to the transport equation is widely used to calculate photon migration in biological tissues, especially for problems with large source and detector separation (Chance and Alfano 1995). For simple geometries analytical solutions exist (Arridge *et al* 1992), and more complex tissues are often modelled with finite-difference (Koo *et al* 1994, Anvari *et al* 1994) or finite-element (Arridge *et al* 1993, Arridge and Schweiger 1995) discretization of the diffusion equation. Also, solutions for the inverse problems of photon migration in biological tissue are almost exclusively based on the diffusion theory approximations (Chance and Alfano 1995). While several studies tested the validity of diffusion theory against Monte Carlo simulations and experiments for small source–detector separation (Star 1989, Flock *et al* 1989, Yoo *et al* 1990, Madsen *et al* 1992, Hielscher *et al* 1995b, Okada *et al* 1996, Firbank *et al* 1996), the accuracy of the diffusion approximation, in large homogeneous and inhomogeneous media, such as the breast or the brain, has yet to be proven. Comparisons with Monte Carlo simulations are virtually

‡ As of 1 April 1998 A H Hielscher is with the final affiliation given above‖. E-mail address: hielsch@lanl.gov

0031-9155/98/051285+18$19.50

impossible in these practical cases. The computation times easily exceed several weeks or months, in situations that involve, for example, 5–10 cm of breast tissue or 10–20 cm of brain tissue.

A fast way of accurately calculating the light distribution in large heterogeneous scattering media is given by the discrete-ordinate finite-difference formulation of the transport equation. While this method for solving the transport equation for arbitrary media was introduced as early as 1950 (Chandrasekhar 1950) and finds a wide range of applications in various fields that deal with the transport equation, e.g. oceanography and atmospheric science (Liou 1973, Vanbauce *et al* 1993, Jin and Stamnes 1994), astronomy (Chick *et al* 1996), neutron physics (Badruzzaman and Chiaramonte 1985, Rhoades and Childs 1991) and medicine (Matsumoto *et al* 1991), it has rarely been used to describe light transport in tissues. The only exception is the work by Rastegar *et al* (1989) who used a discrete-ordinate method that was developed by Houf and Incropera (1980) to calculate the one-dimensional fluence rate distribution in a small, slab-like, homogeneous medium. The calculated fluence rates were used as an input for another code, which determined the one-dimensional temperature profiles in homogeneous tissue before onset of ablation caused by laser irradiation.

To calculate three-dimensional fluence rates in large homogeneous and heterogeneous biological tissues, we use in this study a time-independent, discrete-ordinate, finite-difference transport code called DANTSYS that was developed by Alcouffe and co-workers at the Los Alamos National Laboratory (Alcouffe 1977, 1990, 1993, Alcouffe and O'Dell 1987, Alcouffe *et al* 1995). Other than Houf's code, this algorithm makes use of the diffusion synthetic acceleration (DSA) method for the iterative solution of the finite-difference transport equation. As will be shown, the first iteration provides a finite-difference diffusion solution, while the fully converged results equal the finite-difference transport solution. Therefore, diffusion and transport results can be effectively compared, and the validity of the diffusion approximation in large homogeneous and heterogeneous media can be evaluated. For simple geometries, the results of the finite-difference transport and diffusion calculations are also compared with analytical solutions of the diffusion equation.

First we examine homogeneous media. The influence of the ratio of absorption to transport scattering coefficient (μ_a/μ_s') on the accuracy of the diffusion approximation is quantified. This is followed by a discussion of various definitions of the diffusion coefficient, D. Thereafter, heterogeneous media are investigated. We address in detail heterogeneities in which the absorption is comparable with the scattering (e.g. blood vessels and haematoma), and regions that are almost scattering and absorption free (e.g. ventricles in the brain). Finally, we use the knowledge gained from these studies to analyse light transport in the brain. Based on density maps generated by MRI scans, we identify different tissues, assign optical properties and perform diffusion and transport simulations.

2. Theoretical background

2.1. Finite-difference transport code

The migrations of photons in biological tissues can be described by the time- and energy-independent equation of radiative transport, also known as the Boltzmann transport equation:

$$\boldsymbol{\Omega}\cdot\nabla\Psi(\boldsymbol{r},\boldsymbol{\Omega})+(\mu_a(\boldsymbol{r})+\mu_s(\boldsymbol{r}))\Psi(\boldsymbol{r},\boldsymbol{\Omega})=S(\boldsymbol{r},\boldsymbol{\Omega})+\mu_s(\boldsymbol{r})\int_{4\pi}\Psi(\boldsymbol{r},\boldsymbol{\Omega}')\,p(\boldsymbol{\Omega}\cdot\boldsymbol{\Omega}')\,\mathrm{d}\boldsymbol{\Omega}'. \tag{1}$$

Here $\boldsymbol{r}$ is the position vector and $\boldsymbol{\Omega}$ a unit vector pointing in the direction of photon propagation. $\Psi(\boldsymbol{r}, \boldsymbol{\Omega})$ is the energy radiance in units of W cm^{-2} sr^{-1}. The source term $S(\boldsymbol{r}, \boldsymbol{\Omega})$ represents power injected into a solid angle centred on $\boldsymbol{\Omega}$ in a unit volume at $\boldsymbol{r}$. The absorption and scattering coefficients μ_a and μ_s are the inverse of the mean free path (mfp) for absorption and scattering respectively. The phase function $p(\boldsymbol{\Omega} \cdot \boldsymbol{\Omega}')$ describes the probability that during a scattering event a photon with direction $\boldsymbol{\Omega}'$ is scattered in the direction $\boldsymbol{\Omega}$.

The goal of any algorithm that solves equation (1) is to determine $\Psi(\boldsymbol{r}, \boldsymbol{\Omega})$, or the derived parameter

$$\Phi(\boldsymbol{r}) = \int_{4\pi} \Psi(\boldsymbol{r}, \boldsymbol{\Omega})\, \mathrm{d}\boldsymbol{\Omega} \tag{2}$$

which is the energy fluence rate with units of W cm^{-2}. In order to use finite-difference methods for solving equation (1), the spatial variable $\boldsymbol{r}$ and the directional variable $\boldsymbol{\Omega}$ need to be discretized.

In this work we use a finite-difference discrete-ordinate radiative transport code called DANTSYS (diffusion accelerated neutral particle transport code system) that was originally developed to calculate neutron transport in nuclear materials. The spatial discretization is performed by a diamond differencing scheme, also called the Crank–Nicolson method (Alcouffe 1993, Press *et al* 1992). For the discretization of the direction or angle the method of discrete ordinates is employed (Carlson and Lathrop 1968, Bell and Glasstone 1970). This method divides the radiation field into a number of discrete directions Ω_m. In this way the transport equation is transformed into a set of coupled integro-differential equations. Each of these equations is further transformed into a linear differential equation by expanding the phase function, $p(\omega = \boldsymbol{\Omega} \cdot \boldsymbol{\Omega}')$, in a series of Legendre polynomials $P_l(\omega)$

$$p(\omega) = \sum_{l=0}^{L} \frac{2l+1}{4\pi} b_l P_l(\omega) \tag{3}$$

and replacing the scattering integral by a quadrature formula. In this work a Gauss–Legendre quadrature was used. The set of linear differential equations is commonly solved iteratively (Alcouffe 1977, Morel 1982).

In nuclear physics the expansion coefficients, b_l, in equation (3) are usually written as $b_l = (\mu_{s,l}/\mu_{s,0})$, where $\mu_{s,0}$ is referred to as the zeroth moment of the scattering coefficient, and $\mu_{s,l}$ is the lth moment of the scattering coefficient. The zeroth moment equals the scattering coefficient used in the biomedical-optics field ($\mu_s = \mu_{s,0}$). For $b_l = g^l$, where g is the anisotropy factor defined in equation (13), it can be shown that equation (3) equals the well known Heney–Greenstein scattering phase function (Welch and van Gemert 1995, pp 144–5).

Another major feature of DANTSYS is the use of the diffusion synthetic acceleration (DSA) method for the iterative solution of the finite-difference transport equation (Alcouffe 1977, 1990, Larsen 1982, McCoy and Larsen 1982). This method employs a corrected diffusion equation to accelerate the convergence of the transport iterations.

To illustrate the method of DSA, throughout this paper we assume isotropic scattering and an isotropic sources for simplicity. However, the scheme also applies to the more general anisotropic problem (see the excellent review on synthetic acceleration methods by Morel (1982)). For the nth iteration the transport equation (equation (1)) is rewritten as

$$\boldsymbol{\Omega} \cdot \nabla \Psi_n^*(\boldsymbol{r}, \boldsymbol{\Omega}) + (\mu_a(\boldsymbol{r}) + \mu_s(\boldsymbol{r}))\Psi_n^*(\boldsymbol{r}, \boldsymbol{\Omega}) = S(\boldsymbol{r}, \boldsymbol{\Omega}) + \mu_s(\boldsymbol{r})\Phi_{n-1}(\boldsymbol{r}). \tag{4}$$

The corrected diffusion equation at the nth iteration can be expressed as (Morel 1982)

$$-\nabla \cdot D(\boldsymbol{r})\nabla \Phi_n(\boldsymbol{r}) + \mu_a(\boldsymbol{r})\Phi_n(\boldsymbol{r}) = S'(\boldsymbol{r}) - R_n(\boldsymbol{r}). \tag{5}$$

Here D is the diffusion coefficient (see equation (14)), and the correction term is

$$R_n(\boldsymbol{r}) = \nabla \cdot \boldsymbol{J}_n^*(\boldsymbol{r}) + \nabla \cdot D(\boldsymbol{r})\nabla\Phi_n^*(\boldsymbol{r}) \tag{6}$$

with

$$\Phi_n^*(\boldsymbol{r}) = \int_{4\pi} \Psi_n^*(\boldsymbol{r}, \boldsymbol{\Omega})\,\mathrm{d}\boldsymbol{\Omega} \tag{7a}$$

and

$$\boldsymbol{J}_n^*(\boldsymbol{r}) = \int_{4\pi} \boldsymbol{\Omega}\Psi_n^*(\boldsymbol{r}, \boldsymbol{\Omega})\,\mathrm{d}\boldsymbol{\Omega}. \tag{7b}$$

It should be pointed out that no approximations are made to obtain equation (5). Furthermore, note that we use the asterisk to indicate quantities calculated using the angular flux Ψ_n^*, while the scalar flux calculated from the corrected diffusion equation is without the star.

The DSA scheme proceeds now as follows: using Φ_{n-1}, known from the previous iteration, we solve equation (4) for Ψ_n^*. This involves one sweep through the space-angle mesh. Then the correction term, R_n, is calculated using equations (6) and (7). In turn, R_n is used to calculate Φ_n from equation (5), which completes one cycle of iteration. Note that for $n = 0$, a logical first guess is obtained by setting $R_{n=0}$ to zero and solving the diffusion equation for Φ_0. Therefore, the first iteration provides the finite-difference diffusion solution. With each successive iteration the R-corrected diffusion solution (equation (5)) becomes a better approximation to the transport solution, so the method can be thought of as a diffusion improvement method. It can be shown (Alcouffe 1977, Morel 1982) that when DSA is carried to completion, the corrected diffusion equation solution (equation (5)) is the same as the transport solution (equation (4)) within a specified convergence criterion. The DSA is most effective in the case of isotropic scattering. For anisotropic scattering higher moments in the Legendre expansions of the phase function are needed, which can slow down the convergence of the transport iterations.

Other features of the code are the arbitrary spatial assignment of scattering coefficients, absorption coefficients and phase function. Furthermore, the user has the choice of various boundary conditions, spherical, cylindrical or rectangular coordinate systems, and the option to solve problems in one, two or three dimensions.

The code is written in FORTRAN 77 and is available for various platforms (CRAY, and Sun, IBM, HP and SGI workstations, see http://www-rsicc.ornl.gov/codes/ccc/ccc5/ccc-547.html and http://www-rsicc.ornl.gov/SOFTWARE.html). The calculations done for this study were performed on a CRAY Y-MP 8/128. Computation times range from several seconds to 30 min depending on the size of the spatial mesh and the degree of angular discretization. For the simulations in this study we typically used 84 angles in 2D simulations and 168 angles in 3D simulations.

2.2. Diffusion theory

The diffusion approximation to the transport equation is obtained by expanding Ψ in spherical harmonics and keeping only the first two terms of the expansion. It can be shown (Case and Zweifel 1967) that the energy radiance may then be written as

$$\Psi(\boldsymbol{r}, \boldsymbol{\Omega}) = 1/4\pi\,\Phi(\boldsymbol{r}) + 3/4\pi\,\boldsymbol{\Omega}\boldsymbol{J}(\boldsymbol{r}). \tag{8}$$

Inserting equation (8) into equation (1) and evaluating the integral yields

$$[\boldsymbol{\Omega} \cdot \nabla + \mu_a(\boldsymbol{r})]\Phi(\boldsymbol{r}) = 4\pi S(\boldsymbol{r}) - [\boldsymbol{\Omega}\nabla + \mu_a(\boldsymbol{r}) + (1-g)\mu_s(\boldsymbol{r})]3\boldsymbol{\Omega}\boldsymbol{J}(\boldsymbol{r}). \tag{9}$$

This equation is reduced to two equations in the two dependent variables Φ and $\boldsymbol{J}$ by once integrating over $\boldsymbol{\Omega}$ and another time multiplying with $\boldsymbol{\Omega}$ and integrating over $\boldsymbol{\Omega}$

$$\mu_a(\boldsymbol{r})\Phi(\boldsymbol{r}) = S(\boldsymbol{r}) - \nabla \boldsymbol{J}(\boldsymbol{r}) \tag{10}$$

$$\nabla\Phi(\boldsymbol{r}) = -3[\mu_a(\boldsymbol{r}) + (1-g)\mu_s(\boldsymbol{r})]\boldsymbol{J}(\boldsymbol{r}). \tag{11}$$

Finally, inserting equation (11) into equation (10) yields the diffusion equation

$$-\nabla(3\mu_a + 3\mu_s')^{-1}\nabla\Phi(\boldsymbol{r}) + \mu_a\Phi(\boldsymbol{r}) = S(\boldsymbol{r}). \tag{12}$$

Notice that in equation (12) the scattering coefficient μ_s has been replaced by the transport scattering coefficient μ_s', which is defined as $\mu_s' = \mu_s(1-g)$, where g is the average of the cosine of the scattering angle, also called the anisotropy factor, given by

$$g := \int_{4\pi} \boldsymbol{\Omega}' \cdot \boldsymbol{\Omega}\, p(\boldsymbol{\Omega}' \cdot \boldsymbol{\Omega})\, \mathrm{d}\boldsymbol{\Omega}'. \tag{13}$$

The inverse of μ_s' can be interpreted as the distance a photon has to travel before it loses all information regarding its initial direction. This distance is also called the reduced or transport mean free path (mfp′).

The diffusion coefficient D is defined as

$$D = (3\mu_a + 3\mu_s')^{-1}. \tag{14}$$

Other definitions of D have recently been proposed ($D = (3\mu_s')^{-1}$ by Furutsu and Yamada (1994) and $D = (\mu_a + 3\mu_s')^{-1}$ by Wang and Jacques (1995)). We will later (see section 4.3) discuss the influence of these alternative definitions on the diffusion solution.

Solutions to the diffusion equation (12) are readily found. For an infinite medium that contains an isotropic point source, with intensity of I_0(W), at $\boldsymbol{r}_0$ one gets

$$\Phi(\boldsymbol{r}, t) = \frac{I_0}{4\pi D}\frac{\exp(-(\mu_a/D)^{1/2}|\boldsymbol{r} - \boldsymbol{r}_0|)}{|\boldsymbol{r} - \boldsymbol{r}_0|}. \tag{15}$$

Hielscher *et al* (1994) and Boas *et al* (1994) gave analytical solutions for an infinite medium that contains a spherical inhomogeneity. From these formulae one can derive solutions for semi-infinite, slab-like and cube-like media by the method of images (Eason *et al* 1978, Patterson *et al* 1989).

2.3. Simulation geometry and boundary conditions

For the transport simulations and diffusion calculations we adapted the following geometry (figure 1): unless otherwise defined, we assume a three-dimensional cube where a point light source is placed on one side of the cube. Inhomogeneities such as spheres with various radii and optical properties are usually centred in the cube. For the finite-difference transport (FDT) and finite-difference diffusion (FDD) simulations this cube is divided into uniform, orthogonal cells. Great care has to be taken to choose the correct grid spacing, h_n, for the finite-difference code. As a rule of thumb adjacent grid points should be separated by less than one transport mean free path. However, in regions with steep changes in the flux, even smaller steps may be appropriate. To avoid grid size effects, we repeated the simulations with decreasing grid sizes until no changes in the results could be observed. Furthermore, the angular discretization has to be fine enough. In this study we typically used 84 angles in 2D simulations and 168 angles in 3D simulations. Larger numbers change the solutions by less than 0.5%.

Vacuum boundary conditions were chosen for the FDT and FDD calculations. No photon that leaves the cube will return to the medium. For the analytical solutions we

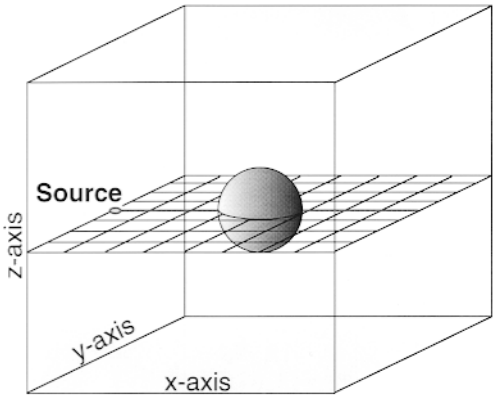

Figure 1. Geometry of problems.

employed the method of images. That is, negative image sources were placed around the cube to ensure the extrapolated boundary condition (Case and Zweifel 1967, Aronson 1995, Hielscher *et al* 1995b).

For the studies on MRI-generated brain data, we assigned different optical properties to grid points with different MRI density levels. In this way the MRI data are segmented into six different areas (skin, skull, grey matter, white matter, cerebrospinal fluid (CSF) and blood).

3. Results

3.1. Homogeneous media

3.1.1. Influence of the ratio μ_a/μ_s'. It is well known that the diffusion approximation requires $\mu_a/\mu_s' \ll 1$. In order to see when and how diffusion theory fails in the case when μ_a/μ_s' approaches 1, we performed a series of simulations and analytical calculations for various values of the ratio. The results are shown in figure 2. In these simulations the scattering coefficient was $\mu_s' = 5.0\ \text{cm}^{-1}$ and $g = 0$. The absorption coefficient was varied from $\mu_a = 0.05\ \text{cm}^{-1}$ to $2.5\ \text{cm}^{-1}$, to yield μ_a/μ_s' ratios from $1/100$ to 1. The mesh spacing for the transport simulations was 0.1 cm, which is half of the scattering length, $1/\mu_s' = 0.2$ cm.

It can be seen that for $\mu_a/\mu_s' = 1/100$, diffusion theory and transport theory yield almost the same result. Small differences near the source can be observed, which are caused by the fact that the analytical solution for a point source has a singularity at $r = 0$, while the finite-difference transport solution has not. For $\mu_a/\mu_s' = 1/10$ diffusion theory underestimates the fluence rate at a distance of 5 cm ($\sim$25 mfp$'$) by almost 35%. For an absorption coefficient of $\mu_a = 2.5\ \text{cm}^{-1}$, $\mu_a/\mu_s' = 1/2$, diffusion theory underestimates the fluence rate at a distance of 25 mfp$'$ by over two orders of magnitude. To ensure that differences between transport and diffusion theory are smaller than 10% at a distance of 25 mfp$'$, we found that μ_a/μ_s' has to be smaller than $1/25$.

The curves in figure 2 show furthermore that with an increasing distance from the source the error increases. This is of importance especially in larger organs, such as the brain or the breast, whose sizes are hundreds of mfps. Even when diffusion theory seems to be a

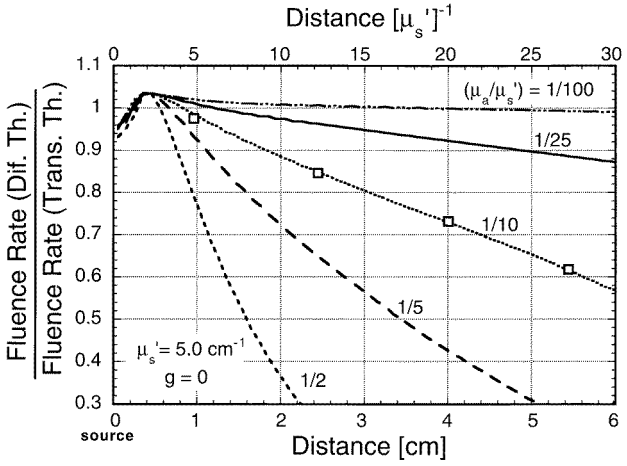

Figure 2. Influence of the ratio μ_a/μ_s' on the accuracy of diffusion theory. The fluence rates for transport theory were calculated with the finite-difference, discrete-ordinate code DANTSYS. The fluence rates for diffusion theory were calculated analytically. The open squares were obtained by using a finite-difference (FD) code to solve the diffusion equation (first DANTSYS iteration).

good approximation because the absorption is smaller than the scattering, the error might get large if measured far away from the source.

In general we can state that the absorption coefficient has to be significantly smaller than the reduced scattering coefficient in order to satisfy the diffusion approximation for large distances from the source. Otherwise, diffusion theory underestimates the fluence rate in the medium, or in other words overestimates the absorption in the medium.

3.1.2. Diffusion coefficient. Recently, it was suggested that diffusion theory can be made more accurate by choosing a different diffusion coefficient, D (Furutsu and Yamada 1994, Yamada 1995, Wang and Jacques 1995). To test this hypothesis we compared finite-difference transport calculations with analytical solutions of the diffusion equation using different definitions of D ($D_1 = (3\mu_a + 3\mu_s')^{-1}$ (see equation (5)), $D_2 = (\mu_a + 3\mu_s')^{-1}$, $D_3 = (0.5\mu_a + 3\mu_s')^{-1}$, $D_4 = (3\mu_s')^{-1}$). For the comparison we chose two homogeneous media with $\mu_s' = 5$ cm^{-1} and $\mu_a/\mu_s' = 1/25$ and $\mu_a/\mu_s' = 1/2$. The results are displayed in figures 3(a) and (b).

In the case of $\mu_a/\mu_s' = 1/25$ (figure 3(a)) it appears that D_3 yields the best agreement between diffusion and transport calculations. Diffusion coefficients D_1 and D_2 yield fluence rates which are increasingly too small as the source–detector separation is increased. D_4 yields fluence rates which are too large.

In the case of $\mu_a/\mu_s' = 1/2$ (figure 3(b)) the calculation with the original diffusion coefficient, D_1, and the newly defined coefficients, D_2 and D_3, all agree with transport theory at some distance from the source ($\sim$3 mfp$'$, $\sim$20 mfp$'$ and $\sim$50 mfp$'$). However, for increasing distance from the source all three diffusion coefficients seem to increasingly underestimate the fluence rate. Furutsu and Yamada's suggestion, D_4, overestimates the fluence rate at all distances; however, the absolute error is smaller than with D_1 at distances larger than 5 mfp$'$. An advantage of choosing D_4 seems to be that the result does not depend as strongly on the distance from the source.

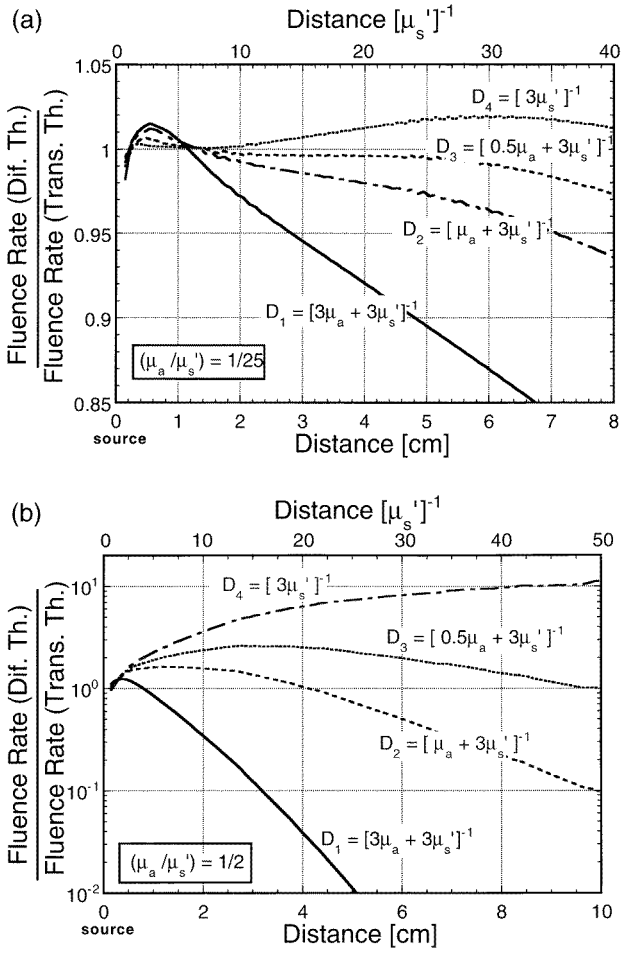

Figure 3. Influence of various definitions of D on the diffusion calculations. The diffusion results were obtained from analytical calculations, while the transport results were determined with DANTSYS. In (a) the ratio $\mu_a/\mu_s' = 1/25$, in (b) the ratio $\mu_a/\mu_s' = 1/2$, with $\mu_s' = 5\ \mathrm{cm}^{-1}$ in both cases.

We found that given a ratio μ_a/μ_s' and a distance between the source and the detector, one can always define a D which gives the same result as the transport equation. However, no general definition of D can be given that fits all situations. Therefore, it appears most prudent to avoid using diffusion theory when it is not valid.

3.2. Heterogeneous media

3.2.1. Influence of μ_a/μ_s'. Next we investigated the differences between diffusion theory and transport theory in heterogeneous media. We first consider a situation that is commonly encountered in blood vessels or haematoma. In the near-infrared wavelength region blood has an absorption coefficient that is comparable with the reduced scattering coefficient (Nilsson 1997, Liu *et al* 1995). Therefore, diffusion calculations are expected to disagree with transport calculations. How light penetrates these heterogeneities is of great interest,

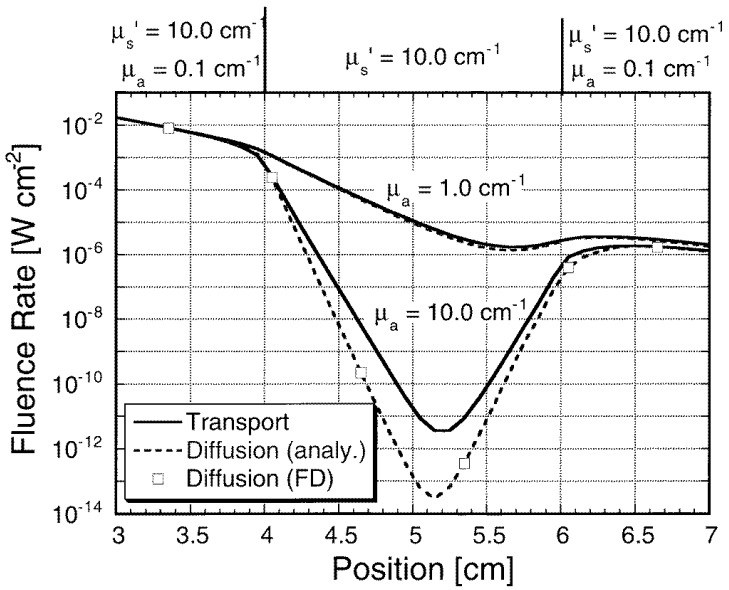

Figure 4. Transport and analytical diffusion calculations of the fluence rates in heterogeneous media with weak ($\mu_a = 1.0$ cm^{-1}) and strong ($\mu_a = 10.0$ cm^{-1}) spherical absorbers. Outside the spherical heterogeneity the absorption coefficient is $\mu_a = 0.1$ cm^{-1}. The scattering coefficient is $\mu_s' = 10$ cm^{-1} throughout the medium. The point source is located at Position $= 0$. The open squares were obtained by using a finite-difference (FD) code to solve the diffusion equation (first DANTSYS iteration).

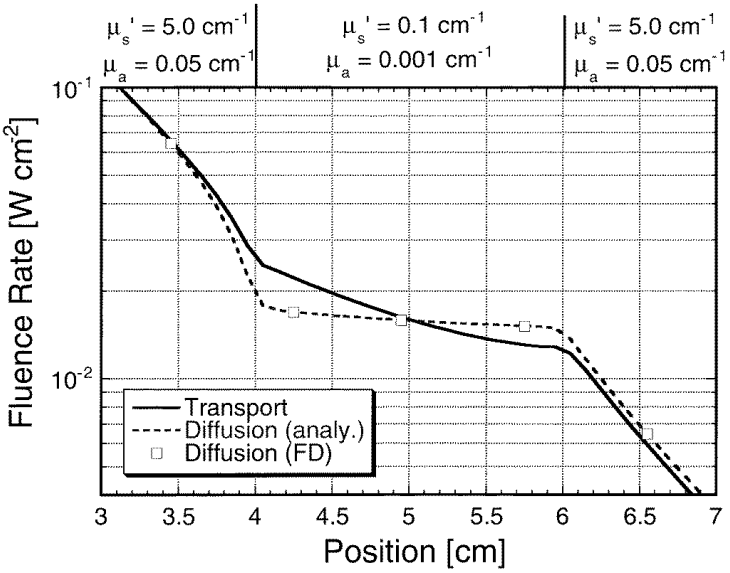

Figure 5. Transport and analytical diffusion calculations of the fluence rates in a medium that contains an almost scattering- and absorption-free sphere ($\mu_s' = 0.1$ cm^{-1}, $\mu_a = 0.001$ cm^{-1}). The optical properties of the surrounding medium are given by $\mu_s' = 5.0$ cm^{-1} and $\mu_a = 0.05$ cm^{-1}. The point source is located at Position $= 0$. The open squares were obtained by using a finite-difference (FD) code to solve the diffusion equation (first DANTSYS iteration).

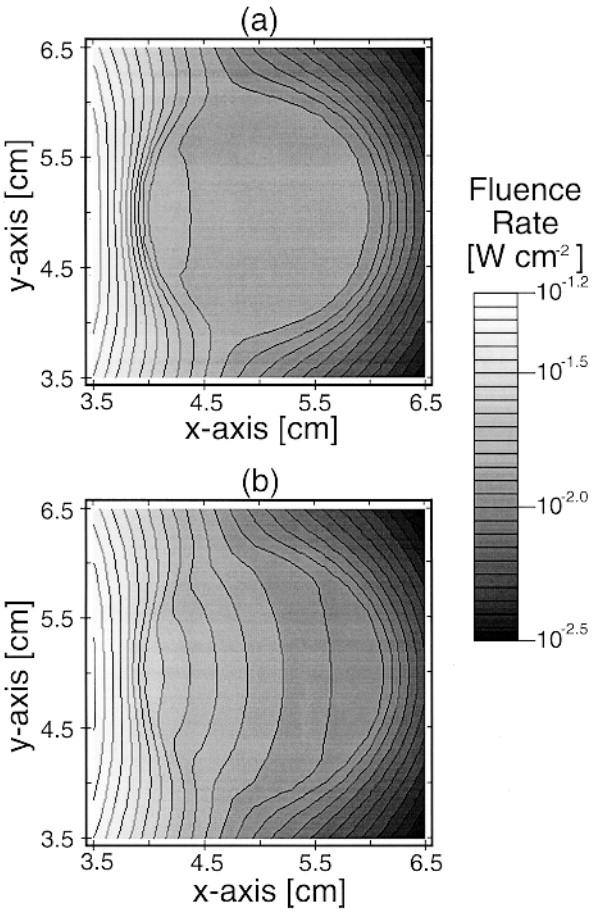

Figure 6. Fluence rates on two-dimensional slices through almost absorption- and scattering-free region: (a) analytical diffusion calculation and (b) finite-difference transport simulations.

for example, in areas where laser induced heating of blood vessels and tissue is used to treat disease (Johnson *et al* 1994, Welch and van Gemert 1995, Sturesson and Andersson-Engels 1996, Gilling *et al* 1996), or in the field of brain haematoma detection (Gophinath *et al* 1993, 1995, Robertson *et al* 1995).

To mimic the influence of blood-filled heterogeneities, we calculated the fluence rate for a $10 \times 10 \times 10$ cm heterogeneous medium that contains a 2-cm-diameter sphere. In figure 4 two kinds of situations are considered. First the spherical heterogeneity has a ten times higher absorption coefficient, $\mu_a = 1.0$ cm^{-1}, than the background medium, $\mu_a = 0.1$ cm^{-1}. The reduced scattering coefficient, $\mu_s' = 10$ cm^{-1}, is the same throughout the medium. As can be seen in figure 4, diffusion and transport theory agree well for this case. However, if μ_a is increased inside the sphere to equal μ_s', large differences between diffusion and transport theory are observed. Diffusion theory overestimates the effect of the heterogeneity by almost two orders of magnitude. On the other hand, the differences occur only inside the sphere. Outside the sphere, the two theories agree rather well.

These results are in agreement with the findings for the homogeneous media. In areas where the ratio of μ_a/μ_s' approaches 1, diffusion theory underestimates the fluence rate in the medium, or in other words overestimates the absorption.

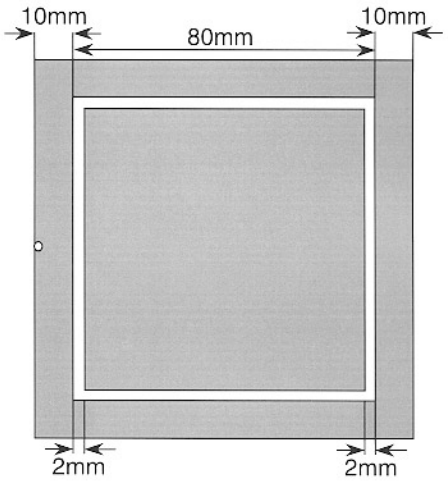

Figure 7. Geometry of channelling problem. Shown is a two-dimensional slice through a three-dimensional cube. In the 2 mm thick, void-like region, which surrounds the $76 \times 76 \times 76$ mm core, the optical properties are $\mu_s' = 0.1$ cm^{-1}, $\mu_a = 0.001$ cm^{-1}. Everywhere else the optical properties are $\mu_s' = 5.0$ cm^{-1} and $\mu_a = 0.05$ cm^{-1}.

3.2.2. Regions with low μ_a and high μ_s'. Of special interest are regions within the body that are almost absorption and scattering free. These regions are for example encountered in the ventricles of the brain, which are filled with cerebrospinal fluid (CSF) (Nolte 1993). Furthermore, a layer of CSF forms a boundary between the skull and the brain. Due to the convoluted nature of the brain, the thickness of the CSF layer varies between about 1 and 10 mm. The effect of such a layer, for example, on measurements of blood oxygenation in the brain has been the subject of many discussions (Hielscher *et al* 1995a, 1996, Firbank *et al* 1996). Other void-like inclusions are, for example, the sinus cavities that surround the nasal cavity. How light propagation is influenced by these near void spaces is discussed next.

Figure 5 shows the results for a medium that contains a spherical heterogeneity with a diameter of 2 cm. The reduced scattering and absorption coefficients within the sphere ($\mu_s' = 0.1$ cm^{-1} and $\mu_a = 0.001$ cm^{-1}) are much lower than in the surrounding medium ($\mu_s' = 5$ cm^{-1} and $\mu_a = 0.05$ cm^{-1}). A continuously emitting light source is located 5 cm from the centre of the inhomogeneity. The fluence rates were analytically calculated with diffusion theory and simulated with the transport code.

Even though the diffusion approximation, $\mu_a/\mu_s' \ll 1$, is valid locally everywhere in the medium, differences between diffusion and transport calculations occur. In the region with very low scattering and absorption the diffusion calculations predict an almost constant fluence rate. Just before this region, diffusion theory predicts a fluence rate smaller than transport theory, and just behind this region, diffusion theory predicts a fluence rate higher than transport theory.

Figures 6(a) and (b) display contours of isofluence rate for a cross section through the same 3D simulation as depicted in figure 5. The plane shown includes an area of 3×3 cm centred in the middle of the 2 cm diameter spherical inhomogeneity. The diffusion calculations predict an almost constant fluence rate throughout the inhomogeneity (figure 6(a)). In contrast, the transport simulation shows a spherical attenuation of the fluence rate within the void (figure 6(b)). This spherical attenuation is expected and is caused by

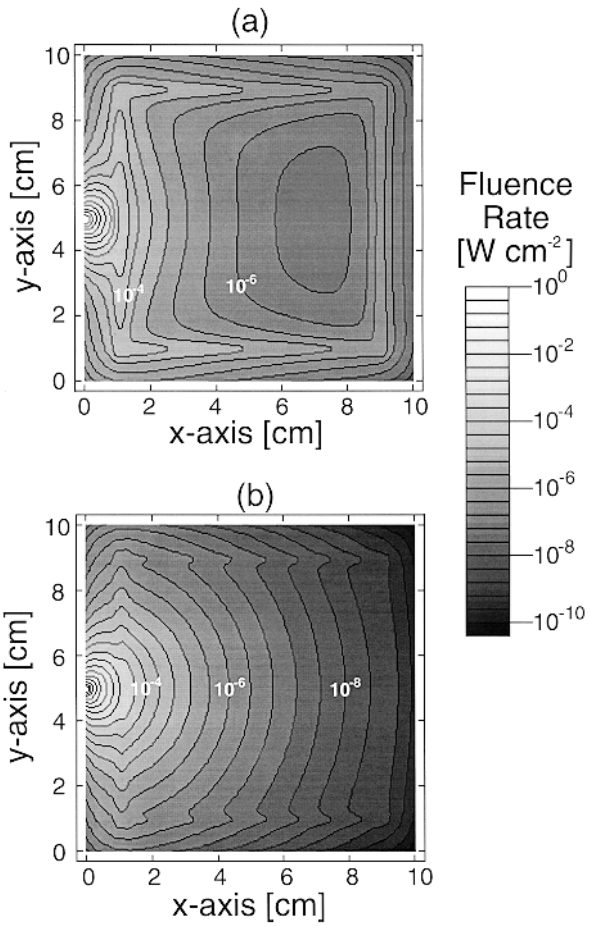

Figure 8. Fluence rates as calculated by the finite-difference diffusion (a) and transport (b) methods for the two-dimensional slice shown in figure 7.

geometrical effects, similar to the spherical attenuation of the electromagnetic field generated by a point source in free space. Although in our case there is not a point source within the low-scattering, low-absorbing region, there is a point, P_h ($x = 4$ cm, $y = 4$ cm), that is closest to the source and has the highest fluence rate. The spherical attenuation in the void-like area originates from this point. Another indication that geometry effects play an important role in light propagation in void-like media is the fact that differences between transport theory and diffusion calculations are largest in 3D simulations and smaller in 2D and 1D. It appears that diffusion theory does not accurately describe attenuations due to geometrical effects.

The failure of diffusion theory to describe the light propagation in low-absorbing and low-scattering media is even more apparent in the following example. As mentioned before, the brain is embedded in an almost absorption- and scattering-free fluid called CSF. To mimic this situation we performed simulations on a $10 \times 10 \times 10$ cm cube with $\mu_s' = 5$ cm^{-1} and $\mu_a = 0.05$ cm^{-1}. The void-like structure ($\mu_s' = 0.1$ cm^{-1} and $\mu_a = 0.001$ cm^{-1}) is this time a 2 mm thick box, which surrounds a $76 \times 76 \times 76$ mm inner cube (figure 7). Figures 8(a)

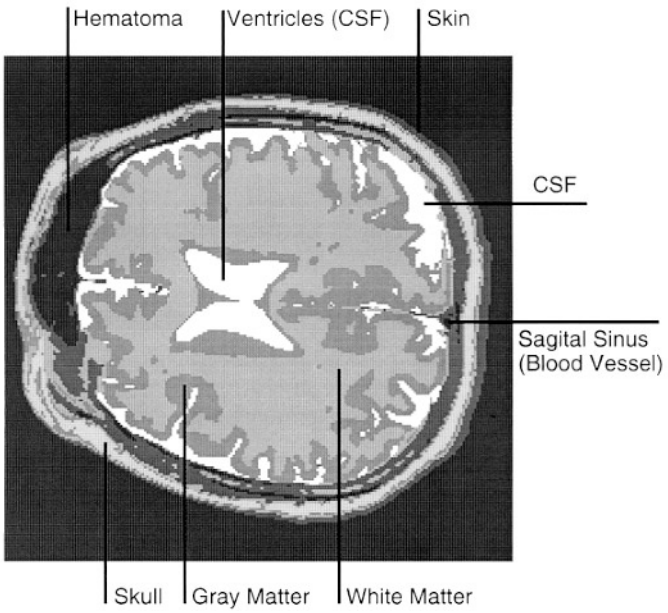

Figure 9. Segmented MRI data for a human brain.

and 8(b) show results of finite-difference diffusion and transport simulations respectively for a plane through the cube, which contains the source on the left. Big differences can be observed, which are caused by a light-channelling effect within the almost clear layer as predicted by diffusion theory. This result confirms the finding of Firbank *et al* (1996), who showed that diffusion theory predicts erroneous backreflections from a turbid medium when a clear subsurface layer is introduced.

3.3. Clinical example

As a final example we took an MRI scan of the brain and segmented it into different areas with various optical properties. MRI imaging techniques allow us to distinguish between fatty white matter, the more watery grey matter, the CSF filled ventricles, the skull, the skin and the blood. These different tissues and fluids appear in an MRI scan with different densities. From this one obtains an optical property map (μ_a, μ_s') by assigning different optical properties to different density values. Figure 9 shows such a segmented scan for a slice that was taken just above the eyebrows through a human head. For example, clearly visible are the butterfly-like ventricles in the centre, which are filled with cerebrospinal fluid (CSF). The optical properties chosen for the different tissues and fluids are representative values for light in the near-infrared (600–900 nm). We chose for white matter $\mu_a = 0.1$ and $\mu_s' = 12$ (Sevick *et al* 1991), grey matter $\mu_a = 0.15$ and $\mu_s' = 6$ (Sevick *et al* 1991, van der Zee *et al* 1993, Bevilacqua *et al* 1995), CSF $\mu_a = 0.01$ and $\mu_s' = 0.1$, skull $\mu_a = 0.05$ and $\mu_s' = 16$ cm^{-1} (Firbank *et al* 1993), skin $\mu_a = 0.2$ and $\mu_s' = 5$ (Hielscher *et al* 1996) and whole blood $\mu_a = 3.0$ cm^{-1} and $\mu_s' = 18$ cm^{-1} (Liu *et al* 1995, Nilsson *et al* 1997).

The results of the two-dimensional, finite-difference transport and diffusion simulations are shown in figures 10(a) and 10(b). The light source is placed on the forehead ($x = 0.4$ cm,

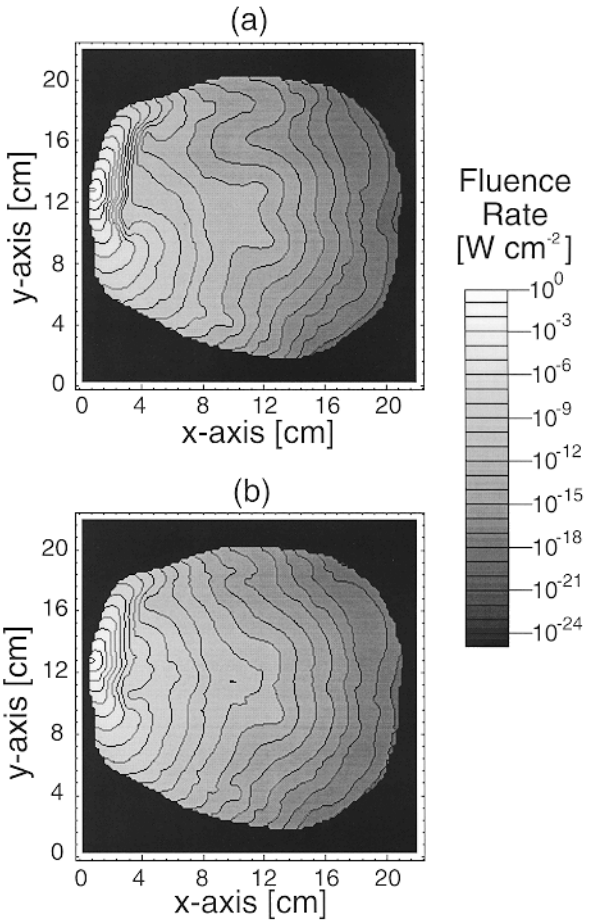

Figure 10. Fluence rates as calculated by the finite-difference diffusion (a) and transport (b) methods for a two-dimensional slice through human brain as shown in figure 9.

$y = 12.8$ cm) just above the haematoma. The different grey values represent different fluence rate levels. The isofluence rate lines indicate a one order of magnitude drop in the fluence rate between two lines.

Several observations can be made that are in agreement with the findings for the phantom problems discussed previously. In the blood filled region of the haematoma (approximately 2.5 cm $< x <$ 3.5 cm and 11 cm $< y <$ 16.5 cm), the isofluence rate lines are much denser in the diffusion case than in the transport calculations. This indicates a much steeper decay of the fluence rate in this region when diffusion theory is used as compared with transport theory. Because μ_a in the haematoma is not much smaller than μ_s', diffusion theory overestimates the absorption effect as discussed in sections 3.1.1 and 3.2.1 and figures 2 and 4.

Differences can also be observed in the region of the ventricles (approximately 8.5 cm $<$ $x <$ 12.5 cm and 8.5 cm $< y <$ 12.5 cm). Diffusion theory predicts a decay of the fluence rate within the ventricles of less than one order of magnitude and the butterfly-like structure is clearly outlined in the 2D diffusion slice. Transport calculations show a decay of over

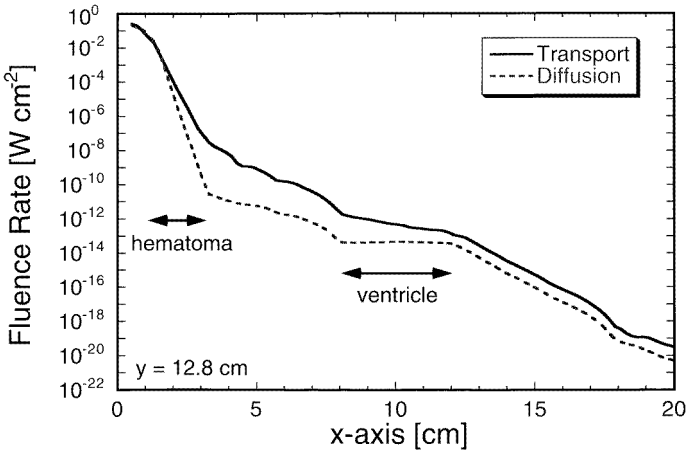

Figure 11. Finite-difference diffusion and transport results of fluence-rate calculations for the line through the human brain shown in figure 9. The line includes the source at $x = 0.4$, $y = 12.8$ (see figure 10), and is parallel to the x-axis.

two orders of magnitude. Since this region is almost free of absorption and scattering, these results agree with the findings in section 3.2.2.

Figure 11 shows the fluence rate on a line that contains the source and crosses through the haematoma and one of the ventricles. Again, the different influences of the haematoma and ventricles on diffusion and transport calculations are clearly visible.

Light channelling can be observed to some extent in the diffusion calculations of the brain. In CSF filled regions, along 6 cm $< x <$ 16 cm, $y = 18$ cm, and 7 cm $< x <$ 10 cm, $y = 4$ cm, the diffusion simulations show an expansion of fluence rate much more pronounced than do the transport calculations.

4. Summary

We used a finite-difference discrete-ordinate transport code to test the limits of diffusion theory in large homogeneous and heterogeneous tissues. Diffusion theory results were obtained by analytical solutions and finite-difference diffusion simulations. For homogeneous media we found that when the diffusion approximation ($\mu_a/\mu_s' \ll 1$) is violated diffusion theory overestimates absorption effects. Diffusion calculations predict for this case a much stronger decay of the fluence rate than do transport calculations. In large media small differences between diffusion and transport theory accumulate and differences can become significant far away from the source, even when $\mu_a/\mu_s' = 1/10$.

As in homogeneous media, diffusion theory overestimates the absorption effects of heterogeneities that contain a material with $\mu_a \sim \mu_s'$. Furthermore, we found that diffusion theory fails to accurately describe regions with very low scattering and absorption coefficients, such as the void-like ventricles in the brain. If these almost scattering- and absorption-free regions form a tunnel-like structure, diffusion theory predicts a channelling of light, while transport theory suggests a decay even within these tunnels due to geometrical light attenuation.

Diffusion and transport calculations also show a large difference if applied to light transport in the human brain. In agreement with the simulations on less complex systems,

diffusion calculations differ most strongly from transport results in highly absorbing regions, such as haematoma, and void-like spaces, such as the ventricles and the subarachnoid space.

Acknowledgments

The authors would like to thank Professor Yao Wang from the Department of Electrical Engineering at Polytechnic University, in Brooklyn, NY for help in handling the MRI data and Dr Scott Walker from Los Alamos National Laboratory for the careful review of the manuscript. This work was supported in part by an NIH grant CA66184-A02 and a fellowship from the director's office at Los Alamos National Laboratory.

References

Alcouffe R E 1977 Diffusion synthetic acceleration: method for the diamond difference discrete ordinates equation *Nucl. Sci. Eng.* **64** 344–52

——1990 A diffusion accelerated S_N transport method for radiation transport on a quadrilateral mesh *Nucl. Sci. Eng.* **105** 191–7

——1993 An adaptive weighted diamond differencing method for three-dimensional xyz geometry *Trans. Am. Nucl. Soc.* **68** 206–12

Alcouffe R E, Baker R S, Brinkley F W, Marr D R, O'Dell R D and Walters W F 1995 DANTSYS: a diffusion accelerated neutral particle transport code system *Los Alamos National Laboratory Manual* LA-12969-M

Alcouffe R E and O'Dell R D 1987 Transport calculation for nuclear analyses: theory and guidelines for effective use of transport codes *Los Alamos National Laboratory Report* LA-10983-MS

Anvari B, Rastegard S and Motamedi M 1994 Modeling of intraluminal heating of biological tissue: implications for treatment of bening prostatic hyperplasia *IEEE Trans. Biomed. Eng.* **41** 854–64

Aronson R 1995 Boundary conditions for diffusion of light *J. Opt. Soc. Am.* A **12** 2532–9

Arridge S R, Cope M and Delpy D T 1992 The theoretical basis for the determination of optical pathlengths in tissue: temporal and frequency analysis *Phys. Med. Biol.* **37** 1531–60

Arridge S R and Schweiger M 1995 Photon-measurement density-functions 2: finite-element-method calculation *Appl. Opt.* **34** 8026–37

Arridge S R, Schweiger M, Hiraoka M and Delpy D T 1993 A finite-element approach for modeling photon transport in tissue *Med. Phys.* **20** 299–309

Badruzzaman A and Chiaramonte J 1985 A comparison of Monte Carlo and discrete ordinates methods in a 3-dimensional well-logging problem *Trans. Am. Nucl. Soc.* **50** 265–7

Bell G I and Glasstone S 1970 Discrete ordinates and discrete S_N methods *Nuclear Reactor Theory* (New York: Van Nostrand Reinhold) pp 214–51

Bevilacqua F, Marquet P, Depeursinge C and de Haller E B 1995 Determination of reduced scattering and absorption coefficients by a single charge-coupled-device array measurement, part II: measurements on biological tissue *Opt. Eng.* **34** 2064–9

Boas D A, O'Leary M A, Chance B and Yodh A G 1994 Scattering of diffuse photon density waves by spherical inhomogeneities within turbid media: analytical solution and applications *Proc. Natl Acad. Sci. USA* **91** 4887–91

Carlson B G and Lathrop K D 1968 Transport theory—the method of discrete ordinates *Computational Methods in Reactor Physics* ed H Greenspan, C N Kelber and D Okrent (New York: Gordon and Breach) pp 171–270

Case K M and Zweifel P F 1967 *Linear Transport Theory* (Reading, MA: Addison-Wesley)

Chance B and Alfano R R (ed) 1995 Optical tomography, photon migration, and spectroscopy of tissue and model media: theory, human studies, and instrumentation, parts 1 and 2 *Proc. SPIE* **2389**

Chandrasekhar S 1950 *Radiative Transfer* (New York: Academic)

Chick K M, Pollack J B and Cassen P 1996 The transport of thermal radiation in a prostellar envelope *Astrophys. J.* **461** 956–71

Eason G, Nioka S, Nisbet R and Turnbull F 1978 The theory of the backscattering of light by blood *J. Phys. D: Appl. Phys.* **11** 1463–79

Firbank M, Arridge S R, Schweiger M and Delpy D T 1996 An investigation of light transport through scattering bodies with non-scattering regions *Phys. Med. Biol.* **41** 767–83

Firbank M, Hiraoka M, Essenpreis M and Delpy D T 1993 Measurement of the optical properties of the skull in the wavelength range 650–950 nm *Phys. Med. Biol.* **38** 503–10

Flock S T, Patterson M S, Wilson B C and Wynman D R 1989a Monte Carlo modeling of light propagation in highly scattering tissues I: model predictions and comparison with diffusion theory *IEEE Trans. Biomed. Eng.* **36** 1162–8

Furutsu K and Yamada Y 1994 Diffusion approximation for a dissipative random medium and the applications *Phys. Rev.* E **50** 3634–40

Gilling P J, Cass C B, Cresswell M D, Malcolm A R and Fraundorfer M R 1996 The use of Holmium laser in the treatment of benign prostatic hyperplasia *J. Endourol.* **10** 459–61

Gopinath S P, Robertson C S, Contant C F, Narayan R K, Grossman R G and Chance B 1995 Early detection of delayed traumatic intracranial hematomas using near-infrared spectroscopy *J. Neurosurg.* **83** 438–44

Gopinath S P, Robertson C S, Grossman R G and Chance B 1993 Near-infrared spectroscopic localization of intracranial hematomas *J. Neurosurg.* **79** 43–7

Hebeda K M, Menovsky T, Beek J F, Wolbers J G and van Gemert M J C 1994 Light propagation in the brain depends on nerve fiber orientation *Neurosurgery* **35** 720–2

Hielscher A H, Liu H, Chance B, Tittel F K and Jacques S L 1995a Phase resolved reflectance spectroscopy on layered turbid media *Proc. SPIE* **2389** 248–56

——1995b The influence of boundary conditions on the accuracy of diffusion theory in time-resolved reflectance spectroscopy of biological tissue *Phys. Med. Biol.* **40** 1957–75

——1996 Time-resolved photon emission from layered turbid media *Appl. Opt.* **35** 719–28

Hielscher A H, Tittel F K and Jacques S L 1994 Photon density wave diffraction tomography *OSA Proc. on Advances in Optical Imaging and Photon Migration (OSA Proc. 21)* ed R R Alfano (Washington, DC: Optical Society of America) pp 78–82

Houf W G and Incropera E P 1980 An assessment of techniques for predicting radiation transfer in aqueous media *J. Quant. Spectrosc. Radiat. Transfer* **23** 101–15

Jin Z H and Stamnes K 1994 Radiative transfer in nonuniformly refracting layered media: atmosphere ocean system *Appl. Opt.* **33** 431–42

Johnson D E, Cromeens D M and Price R E 1994 Interstitial laser prostatectomy *Lasers Surg. Med.* **14** 299–305

Koo F C, Schlereth F H, Barbour R L and Graber H L 1994 Efficient numerical method for quantifying photon distribution in the interior of thick scattering media *OSA Proc. on Advances in Optical Imaging and Photon Migration (OSA Proc. 21)* ed R R Alfano (Washington, DC: Optical Society of America) pp 187–92

Larsen E Q 1982 Unconditionally stable diffusion-synthetic acceleration methods for the slab heometry discrete ordinates equation. Part I: theory *Nucl. Sci. Eng.* **82** 47–63

Liou K N 1973 A numerical experiment on Chandrasekhar's discrete-ordinate method for radiative transfer: applications to cloudy and hazy atmospheres *J. Atmos. Sci.* **30** 1303–26

Liu H, Hielscher A H, Chance B, Jacques S L and Tittel F K 1995 Influence of blood vessels on the measurements of hemoglobin oxygenation as determined by time-resolved reflectance spectroscopy *Med. Phys.* **22** 1209–17

Madsen S J, Wilson B C, Patterson M S, Park Y D, Jacques S L and Hefetz Y 1992 Experimental tests of simple diffusion model for the estimation of scattering and absorption-coefficients of turbid media from time-resolved diffuse reflectance measurements *Appl. Opt.* **31** 3509–17

Matsumoto T, Aoki M and Aizawa O 1991 Phantom experiment and calculation for invivo B-10 analysis by prompt gamma-ray spectroscopy *Phys. Med. Biol.* **36** 329–38

McCoy D R and Larsen E W 1982 Unconditionally stable diffusion-synthetic acceleration methods for the slab heometry discrete ordinates equation. Part I: numerical results *Nucl. Sci. Eng.* **82** 64–70

Morel J E 1982 A synthetic acceleration method for discrete ordinates calculations with highly anisotropic scattering *Nucl. Sci. Eng.* **82** 34–46

Nilsson A M, Lucassen G W, Verkruysse W, Andersson-Engels S and Van Gemert M J C 1997 Changes in optical properties of human whole blood in vitro due to slow heating *Photochem. Photobiol.* **65** 366–73

Nolte J 1993 *The Human Brain* (St Louis, MO: Mosby)

Okada E, Schweiger M, Arridge S R, Firbank M and Delpy D T 1996 Experimental validation of Monte-Carlo and finite-element methods for the estimation of the optical path-length in inhomogeneous tissues *Appl. Opt.* **35** 3362–71

Patterson M S, Chance B and Wilson B C 1989 Time resolved reflectance and transmittance for the non-invasive measurement of tissue optical properties *Appl. Opt.* **28** 2331–6

Press W H, Flannery B P, Teukolsky S A and Vetterling W T 1992 *Numerical Recipes in C* (New York: Cambridge University Press)

Rastegar S, Motamedi M, Welch A J and Hayes L J 1989 A theoretical study of the effect of optical properties in laser ablation of tissue *IEEE Trans. Biomed. Eng.* **36** 1180–7

Rhoades W A and Childs R L 1991 A 3-dimensional discrete ordinates neutron photon transport code *Nucl. Sci. Eng.* **107** 397–8

Robertson C S, Gophinath S P and Chance B 1995 A new application for near-infrared spectroscopy: detection of delayed intracranial hematomas after head injury *J. Neurotrauma* **12** 591–600

Schweiger M, Arridge S R, Hiraoka M and Delpy D T 1995 The finite element method for the propagation of light in scattering media: boundary and source conditions *Med. Phys.* **22** 1779–92

Sevick E M and Chance B 1991 Photon migration in a model of the head measured using time- and frequency-domain techniques: potential of spectroscopy and imaging *Proc. SPIE* **1431** 84–96

Sevick E M, Chance B, Leigh J, Nioka S and Maris M 1991 Quantitation of time- and frequency-resolved optical spectra for the determination of tissue oxygenation *Anal. Biochem.* **195** 330–51

Star W M 1989 Comparing the P3-approximation with diffusion theory and with Monte Carlo calculations of light propagation in a slab geometry *SPIE Institute Series 5: Dosimetry of Laser Radiation in Medicine and Biology* (Bellingham, WA: SPIE–The International Society for Optical Engineering) pp 146–54

Sturesson C and Andersson-Engels S 1996 Mathematical modeling of dynamic cooling and preheating, used to increase the depth of selective damage to blood vessels in laser treatment of port-wine stains *Phys. Med. Biol.* **41** 413–28

Vanbauce C, Buriez J C, Dubuisson P and Fouquart Y 1993 Determination of fog optical thickness over northern France using AVHRR imagery *Ann. Geophys. - Atmos. Hydrospheres Space Sci.* **11** 160–72

van der Zee P, Essenpreis M and Delpy D T 1993 Optical properties of brain tissue *Proc. SPIE* **1888** 454–65

Wang L H and Jacques S L 1995 Use of a laser beam with an oblique angle of incidence to measure the reduced scattering coefficient of a turbid medium *Appl. Opt.* **34** 2362–6

Welch A J and van Gemert M J C 1995 *Optical-Thermal Response of Laser-Irradiated Tissue* (New York: Plenum)

Yamada Y 1995 Diffusion coefficient in the photon diffusion equation *Proc. SPIE* **2389** 87–97

Yoo K M, Liu F and Alfano R R 1990 When does the diffusion approximation fail to describe photon transport in random media? *Phys. Rev. Lett.* **64** 2647